

Enhanced production of low energy electrons by alpha particle impact

Hong-Keun Kim¹, Jasmin Titze, Markus Schöffler, Florian Trinter, Markus Waitz, Jörg Voigtsberger, Hendrik Sann, Moritz Meckel, Christian Stuck, Ute Lenz, Matthias Odenweller, Nadine Neumann, Sven Schössler, Klaus Ullmann-Pfleger, Birte Ulrich, Rui Costa Fraga, Nikos Petridis, Daniel Metz, Annika Jung, Robert Grisenti, Achim Czasch, Ottmar Jagutzki, Lothar Schmidt, Till Jahnke, Horst Schmidt-Böcking, and Reinhard Dörner

Goethe-Universität Frankfurt, Institut für Kernphysik, Frankfurt, Germany

Edited by R. Stephen Berry, University of Chicago, Chicago, Illinois, and approved June 9, 2011 (received for review April 6, 2011)

Radiation damage to living tissue stems not only from primary ionizing particles but to a substantial fraction from the dissociative attachment of secondary electrons with energies below the ionization threshold. We show that the emission yield of those low energy electrons increases dramatically in ion–atom collisions depending on whether or not the target atoms are isolated or embedded in an environment. Only when the atom that has been ionized and excited by the primary particle impact is in immediate proximity of another atom is a fragmentation route known as interatomic Coulombic decay (ICD) enabled. This leads to the emission of a low energy electron. Over the past decade ICD was explored in several experiments following photoionization. Most recent results show its observation even in water clusters. Here we show the quantitative role of ICD for the production of low energy electrons by ion impact, thus approaching a scenario closer to that of radiation damage by alpha particles: We choose ion energies on the maximum of the Bragg peak where energy is most efficiently deposited in tissue. We compare the electron production after colliding He^+ ions on isolated Ne atoms and on Ne dimers (Ne_2). In the latter case the Ne atom impacted is surrounded by a most simple environment already opening ICD as a deexcitation channel. As a consequence, we find a dramatically enhanced low energy electron yield. The results suggest that ICD may have a significant influence on cell survival after exposure to ionizing radiation.

radioactivity | momentum spectroscopy

Ionization caused by the impact of a charged particle underlies numerous phenomena found in nature. It explains the occurrence of polar lights in the atmosphere and is responsible for the dangers emanating from radiological material. Furthermore, ionization is a fundamental physical process behind many applications of modern life: It is utilized, for example, in fluorescent tubes or in tumor therapy. Despite its rather broad relevance, the understanding of the dynamics inherent in such ionization processes is far from complete (1). Most of the detailed studies of ion impact ionization are performed for isolated atoms or molecules in the gas phase. The energy introduced by the ionizing projectile is deposited to the system and shared among the energy needed to overcome the binding potential, the emitted electrons' kinetic energy, and to a very small amount the recoiling ion. Unlike in photoionization, where the photon energy and consequently the amount of energy brought into the system can be selected, ion–atom collisions accommodate different energy transfers for each ionization process, leading to a continuous energy spectrum of the emitted electrons. A typical example is shown in Fig. 1 (solid line, solid squares) for single ionization of a neon atom by an impinging helium ion



This continuous distribution of electron energies was believed to not change significantly in case the target atom is located in a

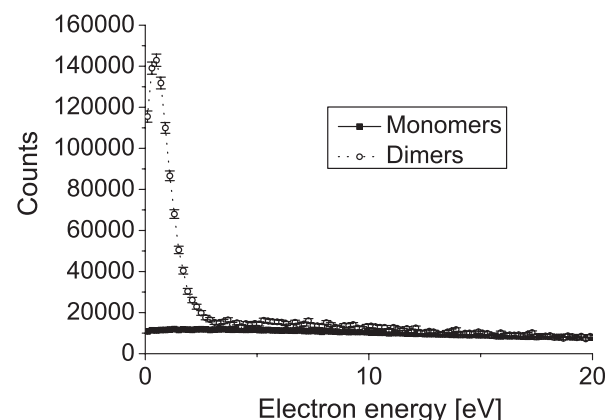


Fig. 1. Electron energy distribution created by 0.65 MeV He^+ ions impinging on neon atoms (solid line, solid squares) and neon dimers (Ne_2) (dotted line, open circles). The two curves are normalized to the same number of target atoms.

chemical environment—i.e., in close proximity of other atoms or molecules. Therefore, these continuous distributions are used as initial electron energy distributions in all computer codes modeling radiation damage. Recently this assumption of an environment having only a minor influence on the ionization process and its reaction products was challenged by the discovery of a new process termed interatomic Coulombic decay (ICD), which is enabled only by the presence of surrounding atoms or molecules. In ICD, first predicted by Cederbaum et al. in 1997 (2), an excited species, typically an ion with a hole in an innervalence shell, relaxes by transferring its excitation energy very efficiently to an atomic or molecular neighbor where it leads to ejection of a low energy electron. The first observation of ICD after its prediction was reported in experiments with Ne clusters (3) and Ne dimers (4) finally proving the existence of ICD. Since then a variety of experiments examining ICD in dimer systems such as He_2 , Ar_2 , Kr_2 , Xe_2 , ArKr , HeNe (5–9) as well as extensive theoretical work (9, 10) was performed. Very recently ICD was even shown to occur in water dimers and clusters (11, 12). Being already discussed in several previous publications (6), these studies finally showed experimentally that there is a rather high possibility that ICD may have a significant impact on radiation damage to living tissue: As ICD occurs in water, it is a source for low energy electrons that is located in the close environment of living tissue. Such

Author contributions: H.-K.K., J.T., M.S., R.G., O.J., T.J., H.S.-B., and R.D. designed research; H.-K.K., J.T., F.T., M.W., J.V., H.S., C.S., U.L., M.O., N.N., S.S., K.U.-P., B.U., R.C.F., N.P., D.M., A.J., and L.S. performed research; H.-K.K., H.S., M.M., and A.C. analyzed data; and H.-K.K., L.S., T.J., and R.D. wrote the paper.

The authors declare no conflict of interest.

This article is a PNAS Direct Submission.

To whom correspondence should be addressed. E-mail: kim@atom.uni-frankfurt.de.

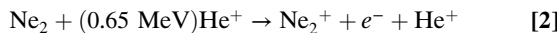
low energy electrons were reported to contribute significantly to the destruction of bio molecules by dissociative attachment to constituents of DNA as, for example, shown in refs. 13 and 14.

All of the above mentioned experiments on ICD, however, were performed by photon impact at synchrotron radiation facilities. A first indication that ICD could be induced by charged particle impact was given in a recent study by Titze et al. (15). They investigated the break-up dynamics of a He_2 after impact with He^{2+} ions in the minor channel of electron transfer to the projectile. In the present article we finally take the studies of ICD to a scenario that more closely resembles that of radiation damage. Radiation damage to tissue is highest at the so called Bragg peak. This is the region along a pathway of an ion through matter where the energy deposited per path length (dE/dx) is maximal. It is, for example, the part of the ion path that is employed in heavy ion cancer therapy in order to destroy tumor cells (16). Therefore, in order to elucidate the relevance of ICD for radiation damage, we investigate the quantitative importance of ICD after ion impact at projectile energies that correspond to the Bragg conditions described above.

As a clean model system we chose the neon dimer Ne_2 , because it offers some particularly advantageous properties as a testbench. Firstly, Ne_2 has been already subject to many experimental and theoretical studies of ICD (4, 17–27) and thus can be regarded as a well known model system for the ICD process. Secondly, it allows us—due to our experimental technique—to directly compare the change in electron emission between an isolated gas phase atom with one that is embedded in an environment: The dimer consists of a neon atom that is surrounded by a single second atom bound only by the van der Waals force (3 meV or 0.07 kcal/mol). Both species—the monomer and the dimer—are simultaneously present in our target beam and can be distinguished from the reaction fragments measured. Therefore, systematical errors are vastly reduced in our approach.

Results

The key result of our work is shown in Fig. 1. It compares the energy distribution of electrons emitted after He^+ impact on Ne , where the neon atom is either isolated or in the environment of another atom as part of a neon dimer. The full line shows a featureless energy spectrum of electrons yielding from ionization processes of the isolated atom as described by Eq. 1. In comparison, the dotted line in Fig. 1 depicts the energy spectrum for electrons created in ion-dimer collisions. The two main processes* contributing to these ion-dimer collisions are described by Eqs. 2 and 3.



For the dimer collisions we observe an enhancement of low energy electrons (below 2.5 eV) by a factor of 14 as compared to the atom. In order to enable a comparison of the absolute occurrences of the ion-atom to ion-dimer channels, the data obtained from our experiment needed to be properly normalized. The two curves are scaled such that they show the yield of electrons per eV emitted for the same total number of target atoms. In the relative normalization of both curves we took an ion detector efficiency of 40% as well as the number of freed electrons into account. As expected, the spectra coincide for higher electron energies. These higher energy electrons are created in a direct interaction of the projectile with one of the Ne atoms, for which a possible environment does not play a major role for the total yield.

*For the studied projectile energy the cross sections for electron capture and electron loss are reported to be orders of magnitude smaller than for ionization (28).

To unravel the mechanism responsible for the dramatic increase in low energy electrons we plot in Fig. 2 the energy correlation between the particles created in ion-dimer collisions. The kinetic energy released (KER), which is the sum of the energy of Coulomb exploding Ne^+ ions (Eq. 3), is plotted against the energy of one of the measured electrons. The color of each bin represents the measured count rate obtained in the experiment. In this histogram events are located in two regions of KER around $\text{KER}_1 = 4.5 \text{ eV}$ and $\text{KER}_2 = 7 \text{ eV}$. Within these two KER areas the electrons are spread continuously over the complete electron energy range with the exception of a dominant diagonal structure within a KER range of 3 eV–5.5 eV ending at about 2.5 eV in electron energy. The events along the diagonal account for 44% of all events in the histogram.

Discussion

Fig. 2 reveals that the high yield of low energy electrons appearing in Fig. 1 for the dotted curve of the dimer ionization originates from that intense diagonal structure. This diagonal corresponds to a constant sum of the electron energy E_e and the KER ($\text{KER} + E_e = 5.35 \text{ eV}$). It is a characteristic of ICD, well known from experiments with synchrotron radiation (4, 26). It results from the decay of an excited state of Ne_2^+ where a 2 s electron is removed from one site of the dimer, which requires an energy of 48.47 eV. The 2 s hole is then filled by a 2p electron from the same site releasing 26.91 eV. This energy is not sufficient to emit a second 2p electron of the now singly charged Ne^+ . Instead a 2p electron (e_{ICD}) of the neighboring neutral Ne atom is ejected for which only 21.56 eV are needed. The energy balance for the overall process thus yields: $48.47 \text{ eV} - 2 \cdot 21.56 \text{ eV} = 5.35 \text{ eV}$. This energy is split among the KER and the $E_{e,\text{ICD}}$ resulting in the observed diagonal.

After the ICD electron has been emitted, the two Ne^+ ions repel each other and fly apart back-to-back. During the breakup the potential energy of $1/R$ (where R is the internuclear distance at the instant of double ionization) is then converted to kinetic energy. Within the reflection approximation (29) the mean internuclear distance of $R_0 = 3.1 \text{ \AA}$ of the neutral Ne_2 (18) corresponds to a $\text{KER} = 4.6 \text{ eV}$, which is close to the observed maximum. This shows that the Neon dimer does not change its geometry much before ICD occurs (this is not true for all systems; see, e.g., refs. 5, 9, and 10).

Furthermore, events located at $3 \text{ eV} < \text{KER} < 5.5 \text{ eV}$ in Fig. 2 that have a higher (continuous) electron energy than 2.5 eV have two sources. Firstly, they result from cases where our detector did not detect the ICD electron but the primary electron emitted from the 2 s shell. Secondly, they originate from another fragmentation route, termed two-step process, observed by Titze et al. in experiments on helium dimers (15). Here the

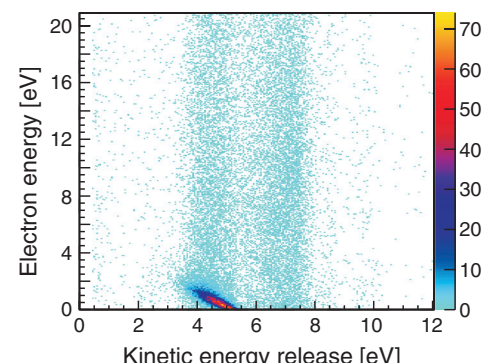


Fig. 2. Correlation of electron and ion energies created by 0.65 MeV He^+ ions impinging on neon dimers (Ne_2) creating two Coulomb exploding Ne^+ ions emitted back-to-back. Horizontal axis: sum energy of both Ne^+ ions (kinetic energy release), vertical axis: energy of the first of the two emitted electrons.

projectile interacts sequentially with both atoms of the dimer. After the ionization of one atom it travels in beam direction, reaching the second site on an attosecond time scale. As soon as the second atom of the dimer is ionized, the dimer will fragment in a Coulomb explosion, which is initiated at the ground state equilibrium distance of the dimer.

The events located at $\text{KER} \approx 7.5 \text{ eV}$ indicate breakups at $R_{\text{KER} \approx 7.5} \approx 1.9 \text{ \AA}$. They result mainly from collisions where the fast projectile doubly ionizes one of the atoms of the dimer. The electrons emitted in this process are both ejected from the 2p shell and show the expected continuous energy distribution. After double ionization, the $\text{Ne}-\text{Ne}^{2+}$ starts to contract as the doubly charged site induces a strong dipole moment. After a lifetime of approximately 100 ps, the two atoms of the dimer approach internuclear distances that are small enough to allow for one electron changing sites. The excess energy gained from this electron exchange is emitted by a photon (24) and finally—as in the other processes observed—the dimer will fragment into two singly charged neon ions.

Another ICD process where a 2 s ionization plus an additional excitation takes place would be located in the same KER region (21). However, this would create an additional diagonal feature that we do not observe. We thus conclude that these additional ICD channels are weak in ion-dimer collisions.

The current results show a substantial contribution of ICD to dimer ionization processes, which leads to a dramatically boosted production of low energy electrons. This finding may be of particular interest to radiobiology. Our experiment was performed at an incident projectile energy of 162.5 keV/u. This energy is close to the maximum of the calculated and, where available, experimentally confirmed stopping power of liquid water for alpha particles (30–32) and therefore likewise corresponds to the peak of the Bragg curve. The Bragg peak, which is utilized in radiotherapy to deposit energy dominantly in tumorous tissue, defines the region with the highest density of ionization thus is fostering ICD as well.

This ultrafast deexcitation mechanism was reported to occur in water clusters, which have equally small binding energies and intermolecular distances as Ne_2 . This suggests a compelling scenario in which alpha radiation significantly induces ICD. The typical energies of electrons being emitted after ICD in water are below 10 eV (11–33). Electrons of this low energy regime were found to be responsible for damages in biomolecules including DNA (an overview of the field is given by ref. 34). Sanche and coworkers determined the yields for single strand and double strand breaks in plasmid DNA films after irradiation with electrons in the energy range of 3–30 eV (13) and 0–4 eV (35). They found significant DNA damages at energies below the ionization and electronic excitation thresholds, which was attributed to dissociative electron attachment: The low energy electron attaches to a DNA subunit (i.e., nucleobase, phosphate deoxyribose backbone, or structural water) leading to the formation of a transient anion. A bond cleavage is induced by the decaying transient anion and hence results in a strand break. A more recent theoretical study (36) predicting a yield of 33% to undergo ICD also after

1. Schulz M, et al. (2003) Three-dimensional imaging of atomic four-body processes. *Nature* 422:48–50.
2. Cederbaum LS, Zobeley J, Tarantelli F (1997) Giant intermolecular decay and fragmentation of clusters. *Phys Rev Lett* 79:4778–4781.
3. Marburger S, Kugeler O, Hergenhahn U, Möller T (2003) Experimental evidence for interatomic Coulombic decay in Ne clusters. *Phys Rev Lett* 90:203401–203404.
4. Jahnke T, et al. (2004) Experimental observation of interatomic Coulombic decay in neon dimers. *Phys Rev Lett* 93:163401–163404.
5. Havermeier T, et al. (2010) Interatomic Coulombic decay following photoionization of the helium dimer: Observation of vibrational structure. *Phys Rev Lett* 104:133401–133404.
6. Morishita Y, et al. (2006) Experimental evidence of interatomic Coulombic decay from the auger final states in argon dimers. *Phys Rev Lett* 96:243402.
7. Lablanquie P, et al. (2007) Appearance of interatomic Coulombic decay in Ar, Kr, and Xe homonuclear dimers. *J Chem Phys* 127:154323.
8. Morishita Y, et al. (2008) Evidence of interatomic Coulombic decay in ArKr after Ar 2p Auger decay. *J Phys B At Mol Opt Phys* 41:025101.
9. Sisourat N, et al. (2010) Interatomic electronic decay driven by nuclear motion. *Phys Rev Lett* 105:173401.
10. Sisourat N, et al. (2010) Ultralong-range energy transfer by interatomic Coulombic decay in an extreme quantum system. *Nat Phys* 6:508–511.
11. Jahnke T, et al. (2010) Ultrafast energy transfer between water molecules. *Nat Phys* 6:74–77.
12. Mucke M, et al. (2010) A hitherto unrecognized source of low-energy electrons in water. *Nat Phys* 6:78–81.
13. Boudaïffa B, et al. (2000) Resonant formation of DNA strand breaks by low-energy (3 to 20 eV) electrons. *Science* 287:1658–1660.
14. Hanel G, et al. (2003) Electron attachment to uracil: Effective destruction at subexcitation energies. *Phys Rev Lett* 90:188104.

Auger decay in water dimers further emphasizes the role of ICD in low energy electron production.

In light of ongoing investigations of ICD in aqueous hydroxide solutions (37) and calculations that predict ICD for broad classes of biomolecules after core hole ionization, and suggest a new therapeutic approach in radiooncology (38), the understanding of basic mechanisms involving ICD is crucial. With the present work we give the first experimental results on the quantitative contribution of ICD to the secondary electron production by ion impact.

Our study shows that by enabling ICD the environment increases the biological effectiveness of ionizing radiation. This counteracts the recently discovered protective role of a solvation shell to biomolecules (39, 40). A detailed understanding of the interplay of these two effects can only be gained in future studies using more complex and possibly aqueous environments than our present rare gas model system.

In conclusion we show that the electron energy distribution of Ne_2 ionization induced by alpha particles differs dramatically from that of electrons emitted from atomic neon. The energy spectrum for electrons originating from Ne_2 fragmentation shows a peak between $0 \text{ eV} < E_{e,\text{ICD}} < 2 \text{ eV}$, exceeding the electron energy spectrum of atomic neon by a factor of 14. We demonstrate that these low energy electrons stem from a fragmentation channel termed ICD that is open only if the ionized particle is located in a chemical environment.

Materials and Methods

The experiment was performed at the 2.5 MV Van-de-Graaff accelerator at the Institut für Kernphysik of the Goethe-Universität in Frankfurt utilizing the COLTRIMS (cold target recoil ion momentum spectroscopy) technique (41–43). The neon dimers are created in a supersonic gas expansion through a 30-μm nozzle that is cooled to 180 K at a driving pressure of 6 bar whereby the fraction of Ne_2 to Ne monomers is estimated to be approximately 1%. Two skimmers with diameters of 0.3 mm and 0.5 mm reduce the target jet area to 1.5 mm perpendicular to its propagation direction. The gas jet is intersected with a He^+ projectile beam that is pulsed at a frequency of 2 MHz and collimated over a distance of 7 m to 0.8 mm × 0.6 mm. Homogeneous weak electric (6.28 V/cm) and magnetic (6.8 Gauss) fields guide the ions and electrons created in the reaction onto two time and position sensitive delay-line detectors (44) with microchannel plates (MCPs), 12 cm in diameter. Two ions and at least one electron were detected. The detected times of flight (TOF) and the positions of the particles were measured in coincidence with the bunch-marker signal of the pulsed projectile beam with a timing resolution of 2.6 ns (FWHM). Hence, for a given spectrometer geometry and known masses, the three dimensional momentum vector at the instant of reaction and the kinetic energy can be determined for each measured particle. The Coulomb explosion of the two recoil ions leads to a unique signature in the TOF of the first ion plotted against the TOF of the second ion. This allows, in addition to momentum conservation, for an efficient suppression of the background created through random events and ionized monomers.

ACKNOWLEDGMENTS. This work was supported by Deutsche Forschungsgemeinschaft. We gratefully acknowledge the excellent preparation of the ion beam by K. Stieberg, P. Ziel, W. Dilfer, and M. Dvorak. We acknowledge discussions on ICD with L. Cederbaum.

15. Titze JN, et al. (2011) Ionization dynamics of helium dimers in fast collisions with He⁺⁺. *Phys Rev Lett* 106:033201.
16. Schulz-Ertner D, et al. (2004) Results of carbon ion radiotherapy in 152 patients. *Int J Radiat Oncol Biol Phys* 58:631–640.
17. Santra R, Zobolev J, Cederbaum LS, Moiseyev N (2004) Interatomic Coulombic Decay in van der Waals Clusters and Impact of Nuclear Motion. *Phys Rev Lett* 85:4490–4493.
18. Wüest A, Merkt F (2003) Determination of the interaction potential of the ground electronic state of Ne₂ by high-resolution vacuum ultraviolet laser spectroscopy. *J Chem Phys* 118:8807–8812.
19. Scheit S, et al. (2004) On the interatomic Coulombic decay in the Ne dimer. *J Chem Phys* 121:8393–8398.
20. Aoto T, et al. (2006) Properties of resonant interatomic Coulombic decay in Ne dimers. *Phys Rev Lett* 97:243401.
21. Jahnke T, et al. (2007) Experimental separation of virtual photon exchange and electron transfer in interatomic Coulombic decay of neon dimers. *Phys Rev Lett* 99:153401.
22. Stoychev SD, Kuleff AI, Tarantelli F, Cederbaum LS (2008) On the interatomic electronic processes following Auger decay in neon dimer. *J Chem Phys* 129:074307.
23. Demekhin PV, Scheit S, Stoychev SD, Cederbaum LS (2008) Dynamics of interatomic Coulombic decay in a Ne dimer following the K-L_{2,3}(¹P) Auger transition in the Ne atom. *Phys Rev A* 78:043421–1–043421–8.
24. Kreidi K, et al. (2008) Relaxation processes following 1 s photoionization and Auger decay in Ne₂. *Phys Rev A* 78:043422.
25. Yamazaki M, et al. (2008) Decay channel dependence of the photoelectron angular distributions in core-level ionization of Ne dimers. *Phys Rev Lett* 101:043004.
26. Kreidi K, et al. (2008) Localization of inner-shell photoelectron emission and interatomic Coulombic decay in Ne₂. *J Phys B At Mol Opt Phys* 41:101002.
27. Kreidi K, et al. (2009) Photo- and auger-electron recoil induced dynamics of interatomic Coulombic decay. *Phys Rev Lett* 103:033001.
28. DuBois RD (1989) Multiple ionization of He⁺-rare-gas collisions. *Phys Rev A* 39:4440–4450.
29. Gislason EA (1973) Series expansions for Franck-Condon factors. I. Linear potential and the reflection approximation. *J Chem Phys* 58:3702–3707.
30. Garcia-Molina R, et al. (2009) Calculated depth-dose distributions for H⁺ and He⁺ beams in liquid water. *Nucl Instrum Methods Phys Res B* 267:2647–2652.
31. Palmer RB (1978) The stopping power of water, water vapour and aqueous tissue equivalent solution for alpha particles over the energy range 05–8 MeV. *J Phys D Appl Phys* 11:605–616.
32. Haque AKMM, Mohammadi A, Nikjoo H (1985) Study of the stopping power and straggling for alpha particles and protons in organic solids, liquids and gases. *Radiat Prot Dosimetry* 13:71–74.
33. Müller IB, Cederbaum LS (2006) Ionization and double ionization of small water clusters. *J Chem Phys* 125:204305.
34. Sanche (2005) Low energy electron-driven damage in biomolecules. *Eur Phys J D* 35:367–390.
35. Martin F, et al. (2004) DNA strand breaks induced by 0–4 eV electrons: The role of shape resonances. *Phys Rev Lett* 93:068101.
36. Stoychev SD, Kuleff AI, Cederbaum LS (2010) On the intermolecular Coulombic decay of singly and doubly ionized states of water dimer. *J Chem Phys* 133:154307.
37. Aziz EF, Ottosson N, Faubel M, Hertel IV, Winter B (2008) Interaction between liquid water and hydroxide revealed by core-hole de-excitation. *Nature* 455:89–91.
38. Schwartz CP, Fatehi S, Saykally RJ, Prendergast D (2010) Importance of electronic relaxation for inter-Coulombic decay in aqueous systems. *Phys Rev Lett* 105:198102.
39. Liu B, et al. (2006) Collision-induced dissociation of hydrated adenosine monophosphate nucleotide ions: Protection of the ion in water nanoclusters. *Phys Rev Lett* 97:133401.
40. Gaigeot MP, et al. (2010) Theoretical investigation of the ultrafast dissociation of ionised biomolecules immersed in water: Direct and indirect effects. *Mutat Res* 704:45–53.
41. Dörner R, et al. (2000) Cold target recoil ion momentum spectroscopy: A ‘momentum microscope’ to view atomic collision dynamics. *Phys Rep* 330:95–192.
42. Ullrich J, et al. (2003) Recoil-ion and electron momentum spectroscopy: reaction-microscopes. *Rep Prog Phys* 66:1463–1545.
43. Jahnke T, et al. (2004) Multicoincidence studies of photo and Auger electrons from fixed-in-space molecules using the COLTRIMS technique. *J Electron Spectrosc Relat Phenomena* 141:229–238.
44. Jagutzki O, et al. (2002) A broad-application microchannel-plate detector system for advanced particle or photon detection tasks: Large area imaging, precise multi-hit timing information and high detection rate. *Nucl Instrum Methods Phys Res A* 477:244–249.